

Crystal Phase-dependent Electrochromic Performance of Porous Titanium Dioxide Nanotube Films

Jian Xiong^{1,2,*}, Anjie Fei¹, Lei Yu¹, Liufen Xia¹, Chu Xu¹, Shengya Chen¹, Guodong Jiang¹, Songdong Yuan¹

¹ Hubei Provincial Key Laboratory of Green Materials for Light Industry, Hubei University of Technology, Wuhan 430068, China

² Collaborative Innovation Center of Green Light-weight Materials and Processing, Hubei University of Technology, Wuhan, 430068 China

*E-mail: 290811086@qq.com

Received: 27 January 2021 / Accepted: 2 March 2021 / Published: 31 March 2021

Electrochromic porous TiO₂ nanotube films with different structural phases were successfully coated on fluorine-doped tin oxide (FTO) glasses by a doctor-blade method with subsequent post-annealing treatment. The TiO₂ crystal phases can be easily tailored via simple post-annealing treatment. The electrochromic performance of coated films was found to be strongly dependent on the TiO₂ crystal phase. An improved optical modulation range was obtained for TiO₂(B) (28.1%) compared to TiO₂ anatase (4.5%) and anatase/TiO₂(B) mixed phases (10%) films by measuring in-situ optical transmittance measurement at 633 nm upon the polarized potential between -0.8V (colored state) and 1.0 V (bleached state). Moreover, the coloration efficiency of pure TiO₂(B) nanotube films reached a value as high as 66.69 cm²/C at 633 nm. These results can be ascribed to the enhanced Li⁺ diffusion coefficient of the TiO₂(B) nanotube film with its open framework structure, which can effectively facilitate the transport of Li⁺ ions during the coloring process. This work demonstrates great potential use of TiO₂(B) films in large-scale electrochromic applications .

Keywords: TiO₂ nanotube films; transmittance spectra; electrochromic performance; Li⁺ diffusion coefficient; TiO₂(B) phase

1. INTRODUCTION

Due to their unique optical tuning characteristics, electrochromic materials (EMs) have attracted extensive attention in the fields of smart windows, electronic displays, information storage, antiglare mirrors, and military usage [1-3]. Typically, EMs can be divided into inorganic electrochromic and organic electrochromic materials [4]. Transitional metal oxides (TMOs) are widely studied as ideal electrochromic materials due to their low cost, excellent thermal stability, and good electrochemical

performance. TMOs can be colored anodically (NiO, V₂O₅) or cathodically (WO₃, TiO₂) with a small polarized voltage [5-6]. Among various TMOs, TiO₂ has received tremendous interest as an excellent cathodic colored material due to its good chemical stability, nontoxicity, and fantastic electrical and optical properties [7-8]. TiO₂ turns blue during the coloration stage in the electrochromic process, and the general electrochromic equation is:



where x is the insertion coefficient of electrochromic activity.

TiO₂ has three distinct polymorphs, known as the anatase, rutile and brookite. However, the electrochromic TiO₂ film presents low optical modulation, poor coloration efficiency, and unsatisfactory electrochemical cycle stability originating from its low ion diffusion coefficient and slow ion and electron transport rates [9]. These drawbacks limit the potential application of TiO₂-based electrochromic films. In the past few years, tremendous work has been devoted to improving the ionic and electronic transport properties, such as precise modification of morphological structure and crystal phase [10-12]. Recently, monoclinic-phase TiO₂(B) has proved to be a very promising anode material for use in Li-ion batteries due to its high insertion capacity and fast ion transport property. The crystal lattice of TiO₂(B) is distinguished by a more open framework structure than the TiO₂ anatase and rutile phases, with facilitating channels for lithium ions fast transport [13]. However, despite numerous works on improving the electrochromic performance of TiO₂, a deep understanding of the electrochromic TiO₂(B)-based films still needs to be explored.

Hence, in this work, titanate nanotube films with different structural phases were successfully coated on FTO substrates by the doctor-blade method; then the TiO₂ films were treated with a subsequent post-annealing process to achieve designed crystal phases. The effect of structure phases on the electrochromic and electrochemical performances was systematically investigated. TiO₂(B) nanotube films exhibited larger optical modulation range, higher coloration efficiency and better electrochemical cycle stability.

2. EXPERIMENTAL

2.1 Synthesis of titanate nanotubes

To prepare titanate nanotubes, a modified two-step hydrothermal approach was used following the process reported in [14]. First, 8 g of TiO₂ powders (Degussa P25) was mixed with 80 mL of 10 M NaOH solution. The mixture was then transferred into Teflon-lined stainless steel autoclaves and was heat at 130° C for 36 h. After that, the obtained product was collected and washed several times until the solution pH value reached about 7. Then the obtained product was mixed with 80 mL of 15 M KOH solution in autoclaves at 200° C for 24 h. The autoclaves were then cooled to room temperature. The final white product was collected and washed several times and neutralized with the appropriate amount of 0.1 M HCl solution, and the remaining traces of NaCl and KCl were removed by sufficient washing with deionized water. The white product was filtered and dried at 60 for 4 h in air. Finally, the product was dispersed in deionized water/Polyethylene Glycol (PEG 20000) mixed solution for use.

2.2 Preparation of TiO₂ films

A doctor blade technique was employed to produce TiO₂ films. First, 90 μ L of prepared titanate product dispersion solution (0.06 g/mL) was scraped on clean FTO substrates (25 mm \times 25 mm \times 1.6 mm, 14 Ω / sq, Wuhan Lattice Solar Energy Technology Co., Ltd.) and then dried to remove water. Then, the obtained films were calcined at 400 ° C, 500 ° C and 600 ° C for 2 h in air. The films were labelled as T-400, T-500 and T-600, respectively.

2.4. Structural, electrochemical and electrochromic characterizations

X-ray diffraction (XRD) patterns of the TiO₂ films were obtained on an X-ray diffractometer (Panalytical X'Pert Pro) equipped with Cu K α radiation ($\lambda=0.15405$ nm). The thickness, surface morphology, microstructure and crystal lattice of the TiO₂ films were characterized by field emission scanning electron microscopy (FESEM, Zeiss, Gemini300) and high-resolution transmission electron microscopy (HRTEM, Tecnai G2 F20). Cyclic voltametric (CV) measurements were performed with a scanning range between -0.8 V and 1.0 V using a potentiostat (CHI750E, CH Instruments). An electrochemical impedance spectrum (EIS, 100 kHz to 1 Hz) was studied using a Zennium IE 6.0 electrochemical workstation containing an Ag/AgCl reference electrode, a platinum counter electrode and TiO₂ film working electrode. LiClO₄+PC (0.5 M) solution was used for the electrolyte for electrochemical tests. In situ optical properties (optical transmittance, coloration efficiency, and switching time) were recorded by combining using a UV-Vis-NIR spectrophotometer (PerkinElmer /Lambda750s) and Zennium IE 6.0 electrochemical workstation. The optical transmittance of the obtained TiO₂ films at a range of 350-1100 nm and the dynamic optical changes at 633 nm under different supplied voltages were measured by a UV-Vis-NIR spectrophotometer.

3. RESULTS AND DISCUSSION

Figure 1 shows the representative HRTEM images of the TiO₂ films calcined at 400 ° C (T-400), 500 ° C (T-500) and 600 ° C (T-600). As depicted in Fig. 1a, uniform one-dimensional nanostructure features comprised typical nanotubes with a length around 100 nm are presented. However, the original nanotube structures partially collapsed and transformed to nanorods upon increasing the calcination temperature to 500°C. Upon increasing the annealing temperature to 600°C, only a few nanotubes can be found, and abundant nanorods and nanoparticles appear. This is well matched with previous research where the titanate nanotubes are easily destroyed and transformed into nanorods and nanoparticles after post-annealing temperatures above than 400°C [15].

As shown in Fig. 1b, the interplanar spacings from nanotubes with $d(200)=0.58$ nm are clearly noticed and can be attributed to TiO₂(B) phase. Since the interplane (200) is parallel to the growth direction of nanotubes, it can be concluded that the nanotubes' preferential growth direction is along the (010) direction. Furthermore, two distinct crystal regions are discerned in Fig. 1d; one still belongs to the TiO₂(B) phase, and the other is ascribed to the TiO₂ anatase phase with $d(101)=0.35$ nm. Fig. 1f

displays only lattice spacings of $d(101)=0.35$ nm for the anatase, indicating that $\text{TiO}_2(\text{B})$ phase no longer exists and was completely transformed into pure anatase with high crystallinity.

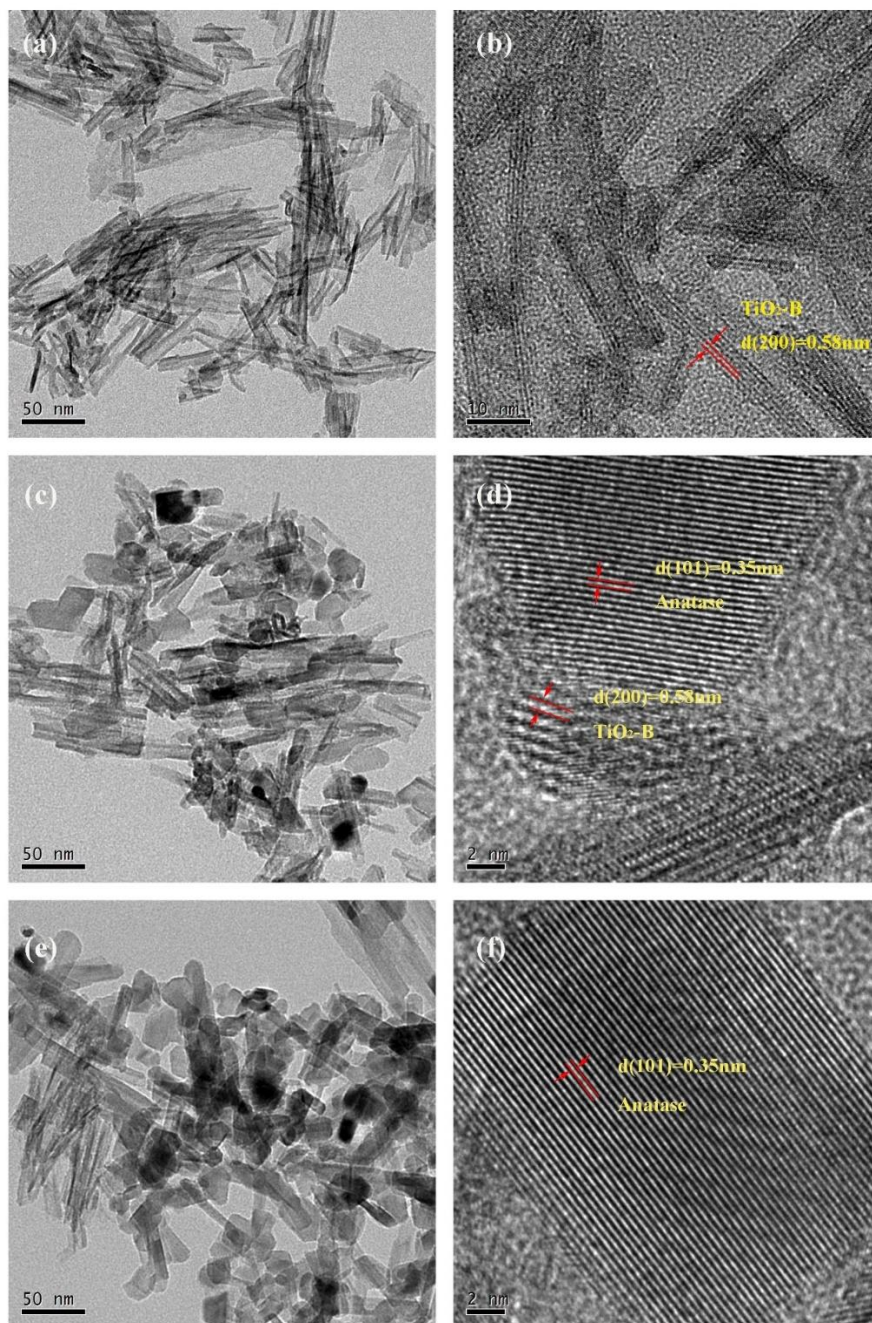


Figure 1. HRTEM images of the TiO_2 films calcined at 400°C (a, b), 500°C (c, d) and 600°C (e, f).

The XRD spectra of the T-400, T-500, and T-600 TiO_2 films are shown in Fig. 2. The diffraction pattern of T-400 shows peaks located at 24.9° , 28.6° and 48.5° that can be well indexed to the $\text{TiO}_2(\text{B})$ phase (JCPDS 46-1237). No other crystal phases were detected, indicating that a complete $\text{TiO}_2(\text{B})$ phase formed. In T-500 and T-600, the peaks located at 25.3° , 37.8° , 48.1° , 53.9° , 55.1° and 62.7° all belong

to the TiO₂ anatase phase (JCPDS 21-1272). A very interesting point to make here is that after carefully analyzing the diffraction patterns of the TiO₂(B) and anatase phases, T-500 showed mixed phases of TiO₂(B) and anatase. Basically, the XRD results demonstrate the gradual crystal phase evolution of TiO₂ films dependent on the post-annealing temperature, which is consistent with the HRTEM information above.

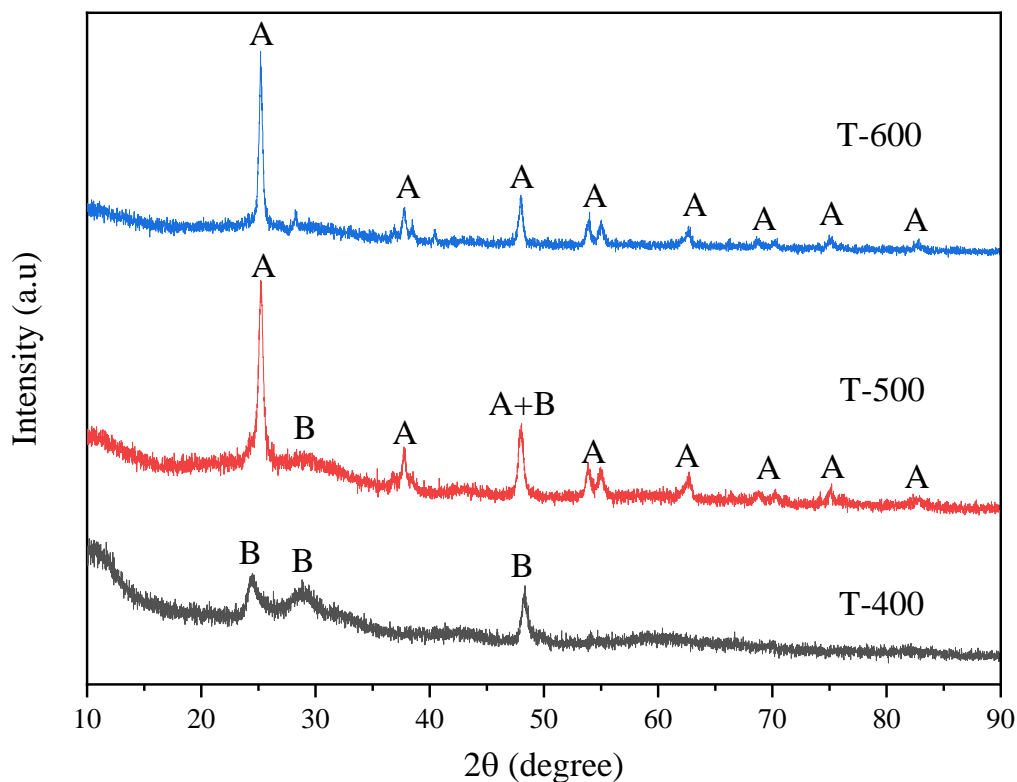


Figure 2. XRD spectra of the TiO₂ films calcined at 400°C, 500°C and 600°C.

The surface morphologies of the T-400, T-500, and T-600 TiO₂ films are shown in Fig. 3. The thickness of the TiO₂ films was examined with a FESEM cross-section technique, where both films were uniform with a thickness around 2 μm. The T-400 film was much more porous and a bit thicker than the T-500 and T-600 films because of its nanotube skeleton, which produced a uniform cross-link framework structure. The surface view images confirm the porous structure of the T-400 film, and the TiO₂ films became dense upon increasing the calcination temperature due to the significant collapse of the nanotube structure.

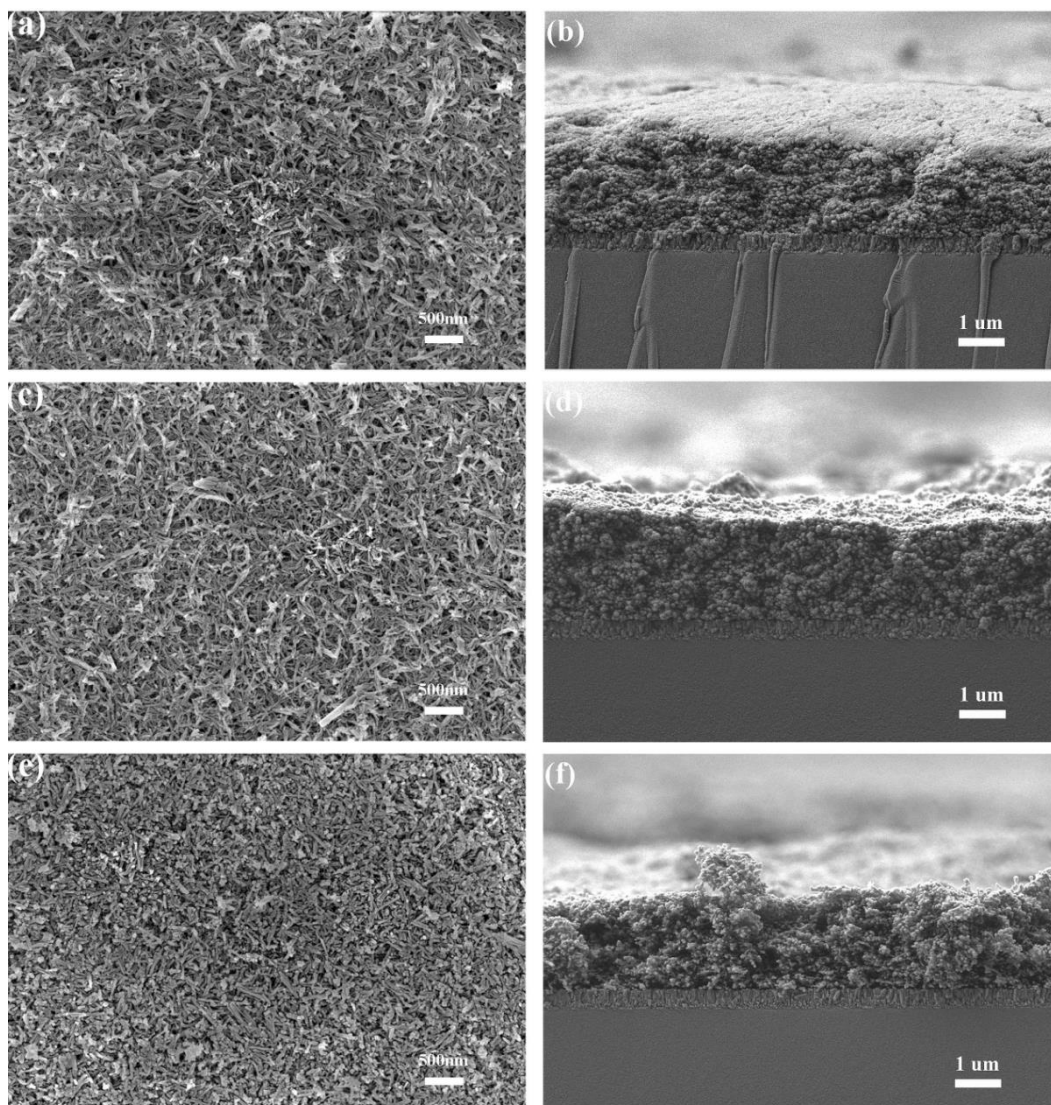


Figure 3. Top-view and cross-sectional FESEM images of the TiO₂ films calcined at 400°C (a, b), 500°C (c, d) and 600°C (e, f).

The optical modulation range is a very important parameter for electrochromic films. Figure 4a shows the optical modulation properties of the T-400 TiO₂ film at different polarized voltages in the range between 350 and 1100 nm. The coloring process starts being activated at a bias voltage of -0.8 V. The T-400 TiO₂ film shows a gradual increase in optical modulation upon increasing the supplied potential from -0.8 V to -1.6 V. Under applied voltages of -0.8 V, -1.0 V, -1.2 V, -1.4 V, -1.6 V, the light modulation amplitudes of the film were 28%, 36%, 46%, 56%, and 63%, respectively. Fig. 4b shows the optical modulation properties of the T-400, T-500, and T-600 TiO₂ films at a bias voltage of -0.8 V in the range between 350 and 1100 nm. As expected, the T-400 TiO₂ film, with its well-formed nanotube structure and TiO₂(B) phase, presents a significantly sharper reduction of the transmittance compared to the T-500 and T-600 TiO₂ films. A huge optical modulation value of 28.1% was reached at a wavelength of 633 nm upon the use of a supplied voltage of -0.8 V, while the T-500 and T-600 TiO₂ films only show 10% and 4.5%, respectively. These results demonstrate that the T-400 film with TiO₂(B)

phase exhibits excellent electrochromic properties even at very low polarized potentials, which can be ascribed to the porous nanotube cross-link structure and TiO₂ (B) phase facilitating fast Li⁺ ion insertion and extraction.

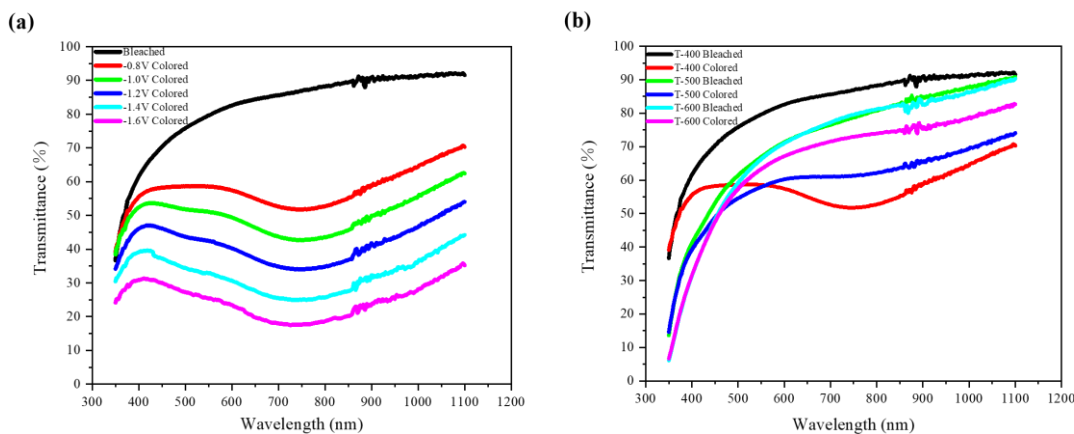


Figure 4. The optical modulation properties of the T-400 TiO₂ film at different polarized voltages (a); the optical modulation ranges of the T-400, T-500, and T-600 TiO₂ films at a fixed bias voltage of - 0.8 V (b).



Figure 5. Picture of the bleached state of the film and the colored state at -1.6 V

The switching properties of the prepared TiO₂ films were also evaluated by monitoring the transmittance in situ at 633 nm by switching the voltage between -0.8 V (colored state) and 1.0 V (bleach state), (as show in Fig. 6). The switching response times are defined as meeting a requirement of a 90% of the total transmittance change. For the T-400 film, the coloration and bleaching response times were 19.4 s and 4.9 s, respectively. We found that the coloring time was much longer than the bleaching time. This is because the coloring/bleaching time is mainly affected by the lithium ion diffusion rate, and the

ion diffusion rate during bleaching is much higher than that during coloring[16]. The switching speed of the T-400 TiO₂(B) film was even faster than those TiO₂ films polarized at higher bias voltages [17].

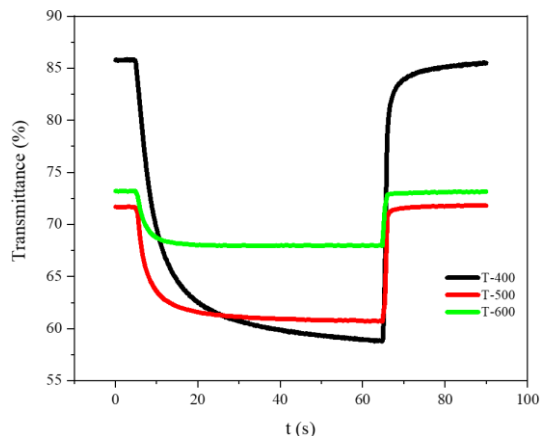


Figure 6. In situ variation of the optical transmittance of the T-400, T-500, and T-600 TiO₂ films measured at 633 nm upon the bias voltage being on/ off.

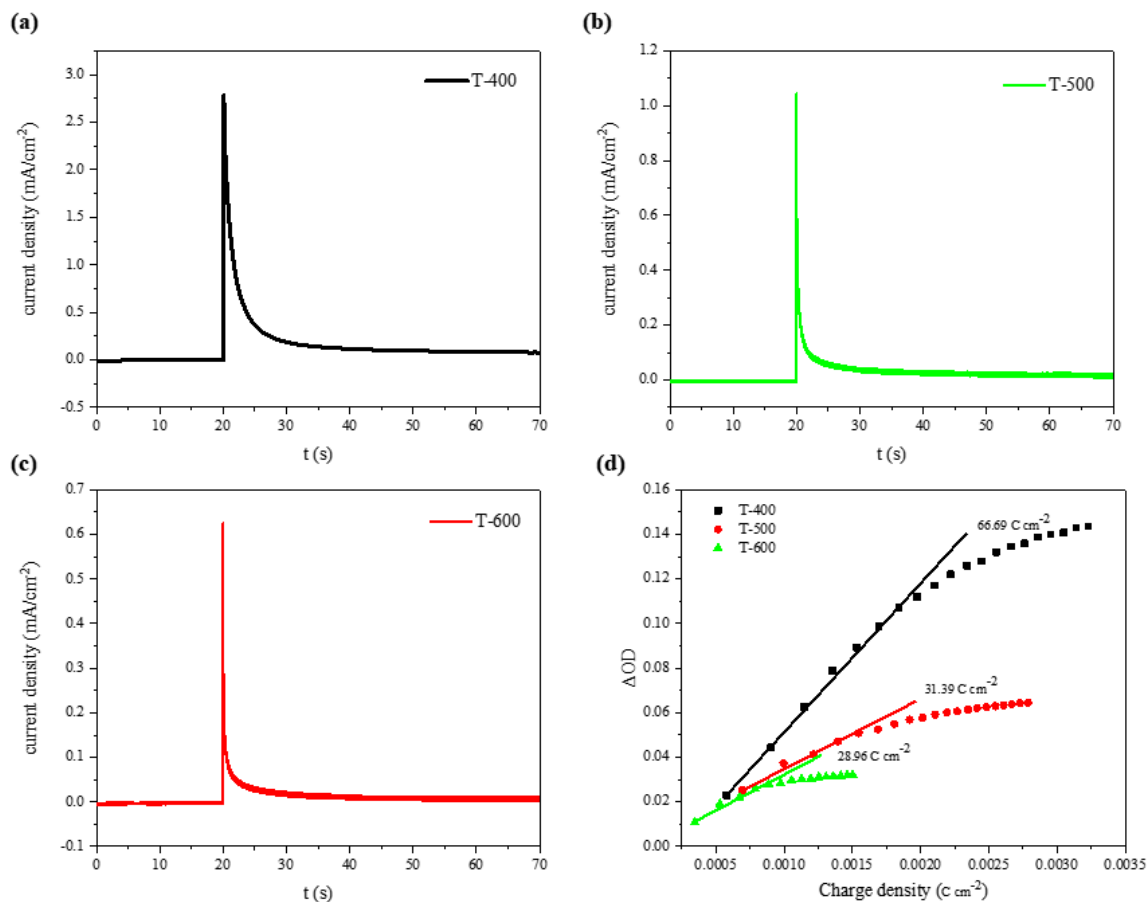


Figure 7. Chronoamperometric curves of (a) T-400, (b) T-500, and (c) T-600 and (d) Variation in the optical density (ΔOD) vs. charge density (Q) for the T-400, T-500, and T-600 TiO₂ films at 633 nm under a bias voltage of -0.8 V.

Another noticeable factor for the electrochromic properties is the coloration efficiency (CE), which is defined as the changes in optical density (ΔOD) per unit of insertion/extract charge for the electrochromic films. The CE value can be calculated by the following equation:

$$CE = \frac{\Delta OD}{Q/A} = \frac{\log\left(\frac{T_b}{T_c}\right)}{Q/A} \quad (2)$$

where T_b and T_c denote the transmittances of the bleached and colored states films, respectively. A is the given working electrode surface area and Q is the integration of the current during the coloring time. Therefore, a high CE value means a small charge density with a large optical modulation [18-19]. Fig. 7d shows the plots of the ΔOD versus the inserted charge density at 633 nm under a polarized voltage of -0.8 V. The calculated CE value for T-400 is 66.69 cm^2/C , which is much larger than T-500 (31.39 cm^2/C) and T-600 (28.96 cm^2/C) or similar products [20]. The superior coloration efficiency of T-400 $\text{TiO}_2(\text{B})$ film is mainly due to its porous and open framework structure, with accessible pores for Li^+ ion diffusion during electrochromic reactions.

Figure 8 shows the coloration/bleaching cycle stability of T-400 $\text{TiO}_2(\text{B})$ film under -0.8 V bias voltage. The optical modulation range decreased from 28.1% to 17% after 200 cycles, still maintaining at 60% of its initial state, indicating a good long-term stability. After 20 cycles of our equipment, the light modulation amplitude dropped to 16% and stabilized. There are many reasons for the reduction of the light modulation amplitude during the cycle of electrochromic film. We attribute the decrease in the light modulation amplitude to the fact that the ions injected into the electrochromic film are not released [21-22]. This good cycle stability is due to the unique open framework structure and well distributed nanotube cross-link structure of $\text{TiO}_2(\text{B})$ phase films, which is beneficial for Li^+ ion transportation.

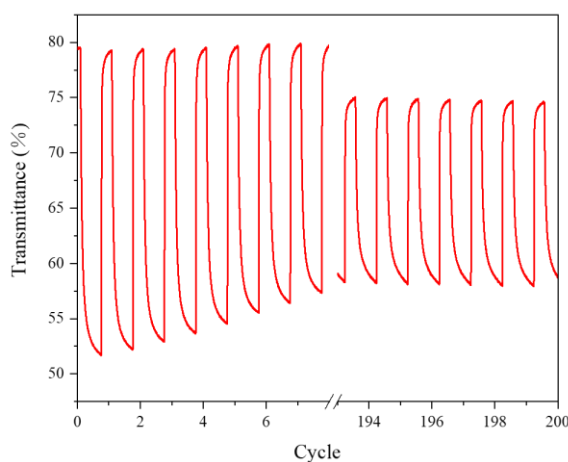


Figure 8. Coloring/ bleaching cycle curves of the T-400 $\text{TiO}_2(\text{B})$ film.

To clarify the insertion/extraction process of Li^+ ions during the electrochromic reaction of the T-400, T-500, and T-600 TiO_2 films, CV measurements were performed with a scan rate of 0.05 V/s in the voltage range of -0.8 to 1.0 V, as shown in Fig. 9a. The CV redox peak areas of the T-400, T-500, and T-600 TiO_2 films decreased with increased calcination temperatures, which can be ascribed to the crystal

lattice deformation of TiO₂, as predicted by the HRTEM and XRD results above. Moreover, it can be found that both the cathodic and anodic current densities of T-400 film are greater than the T-500, and T-600 TiO₂ films, indicating that more Li⁺ ions and electrons were involved in the reaction interface between TiO₂(B) and electrolyte during the electrochromic process. It is well known that the crystal lattice of TiO₂(B) phase has a more open framework structure than anatase, rutile, and brookite phases, which can facilitate the fast transport of Li⁺ ions in the films. The values for charge intercalation (Q_c) and de-intercalation (Q_a) were calculated by integrating the anodic and cathodic peak current densities during the redox process. In T-400 film, the calculated Q_c and Q_a were 0.23 mC/cm² and 0.08 mC/cm², the Q_c and Q_a of T-500 film were 0.15 mC/cm² and 0.043 mC/cm², and the Q_c and Q_a of T-600 film were 0.14 mC/cm² and 0.012 mC/cm². The reversibility during the insertion/extraction reactions can be checked by the ratio of charge densities (Q_a/Q_c), and the Q_a/Q_c values were 0.35 (T-400), 0.29 (T-500), and 0.09 (T-600). These results indicate that more Li⁺ ions can be involved in the insertion/extraction process and better reversibility can be achieved in T-400 TiO₂(B) film. In addition, the results also show that TiO₂(B) film has much better electrochemical reaction activity, which could account for its excellent electrochromic performance even at a low bias potential.

In addition, the Li⁺ ion diffusion coefficient can be calculated from the famous Randles-Sevcik equation :

$$i_p = 2.6 \times 10^5 n^{3/2} A D^{1/2} C v^{1/2} \dots\dots\dots(3)$$

Here, n is the number of transfer electrons (assumed to be 1), i_p is the peak current (A), D is the Li⁺ ion diffusion coefficient (cm²/s), A is the electrode surface area (cm²), C is the activated ions concentration (mol/cm³), and v is the potential scan rate (V/s). Thus, the Li⁺ ion diffusion coefficient of T-400, T-500, and T-600 is 8.3×10⁻¹⁰ cm²/s, 3.1×10⁻¹⁰ cm²/s and 1.4×10⁻¹⁰cm²/s, respectively. The T-400 TiO₂(B) film exhibited much better Li⁺ ion diffusion capability. This is consistent with the EIS results as shown in Fig. 9b.

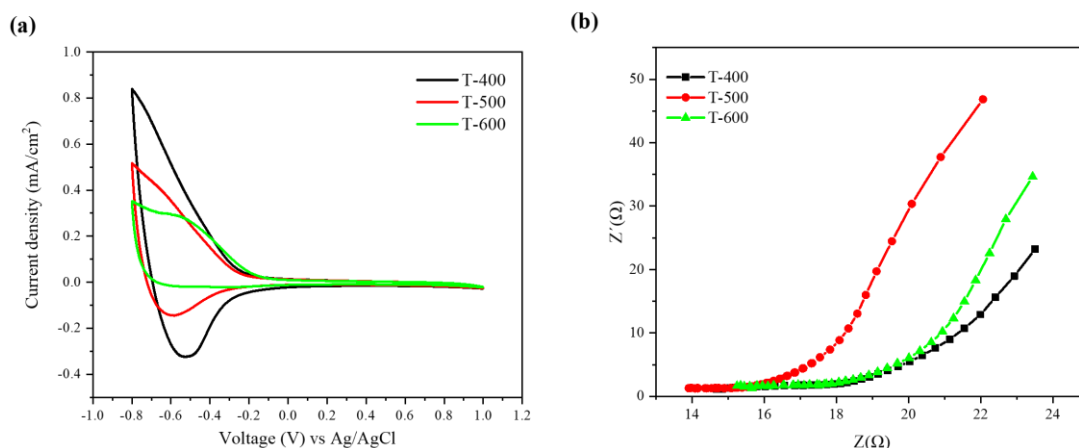


Figure 9. CVs with scan sweep of 50 mV s⁻¹ (a) and EIS (b) of the T-400, T-500, and T-600 TiO₂ films.

The EIS measurements were conducted in the range of 1-100 kHz to evaluate the influence of the TiO₂ crystal phase on the ion transport kinetics during the coloring process. The Nyquist plots of both TiO₂ films consist of a small semicircle in the high frequency region and an inclined line in the low frequency region, which are related to charge transfer resistance and ion diffusion resistance,

respectively. It is well known that a line with higher slope indicates lower ion diffusion coefficient [23-24]. The T-400 TiO₂(B) film showed an enhanced Li⁺ ions diffusion rate, which is consistent with the ion diffusion coefficient calculations above.

4. CONCLUSIONS

Electrochromic porous TiO₂ nanotube films with different crystal phases were successfully coated on FTO substrates by the doctor-blade method combined with a subsequent post-annealing process. The prepared TiO₂ films were transparent in the visible range and well colored in an electrolyte solution of 0.5 M LiClO₄ in PC. It was found that TiO₂(B) phase film, with a well-ordered nanotube structure, has a superior electrochromic performance even at -0.8 V bias voltage. The in situ optical transmittance, measured at 633 nm by supplying the polarized potential between -0.8V (colored state) and 1.0 V (bleached state), indicates that the improved optical modulation range was obtained for TiO₂(B) (28.1%) compared to TiO₂ anatase (4.5%) and anatase/TiO₂(B) mixed phase (10%) films. The coloration efficiency of pure TiO₂(B) nanotube films reached a value as high as 66.69 cm²/C at 633 nm. These results can be ascribed to the enhanced Li⁺ diffusion coefficient of TiO₂(B) with its open framework structure, which facilitates the fast transport of Li⁺ ions during the coloring process. Hence, this work suggests that the TiO₂(B) nanotube films are potential candidates for various electrochromic applications.

DISCLOSURE STATEMENT

No potential conflict of interest was reported by the authors.

FUNDING

This work is supported by the National Natural Science Foundation of China (No. 51901072).

References

1. H. Wang, C.J. Yao, H.J. Nie, L. Yang, S. Mei and Q. Zhang, *J. Mater. Chem. C.*, 44 (2020) 15507.
2. H.X. Jia, X. Cao and P.S. Jin, *J. Inorg. Mater.*, 35 (2020) 511.
3. W. Wei, M. Wang, J. Ma, Y. Cao and Y. Deng, *Adv. Electron., Mater.* 4 (2018) 1800185.
4. S. Xiong, S. Yin, Y. Wang, Z. Kong, J. Lan, R. Zhang, M. Gong, B. Wu, J. Chu and X. Wang, *Mater. Sci. Eng. B-Adv.*, 221 (2017) 41.
5. H. Li, L. Mcrae, A.Y. Elezzabi, *ACS Appl. Mater. Inter.*, 10 (2018) 10520.
6. T. Katase and H. Ohta, *Semicond. Sci. Tech.*, 34 (2019) 123001.
7. N. Akkurt, S. Pat, R. Mohammadigharehbagh, M. Zgür and A. Korkmaz, *J. Mater. Sci - Mater. El.*, 31 (2020) 9568.
8. Nunes, Freire, Barranger, Vieira and Martins, *Appl. Sci. Basel.*, 10 (2020) 1200.
9. C. Hua, G. Yuan, Z. Cheng, H. Jiang, G. Xu, Y. Liu and G. Han, *Electrochim. Acta.*, 309 (2019) 354.
10. Z. Tong, S. Liu, X. Li, J. Zhao and Y. Li, *Nanoscale Horiz.*, 3 (2018) 261.
11. X. Lv, X. Xu, Y. Zhang, D.S. Wright, Y. Zhang and C. Zhang, *Nanotechnology.*, 31 (2020) 355201.
12. H. Xu, L. Gong, S. Zhou, K. Cao, S. Wang, J. Zhao and Y. Li, *New J. Chem.*, 44 (2020) 2236.
13. R. Giannuzzi, M. Manca, L.D. Marco, M.R. Belviso, A. Cannavale, T. Sibillano, C. Giannini, P.D. Cozzoli and G. Gigli, *Chem. Eng. J.*, 6 (2014) 1933.

14. C. Wang, X. Zhang, Y. Wei, L. Kong, F. Chang, H. Zheng, L. Wu, J. Zhi and Y. Liu, *Dalton T.*, 44 (2015) 13331.
15. K. Kiatkittipong, J. Scott and R. Amal, *ACS Appl. Mater. Inter.*, 3 (2011) 3988.
16. Y. Zhu, M.T. Otlej, F.A. Alamer, A. Kumar, X. Zhang, D. Mamangun, M. Li, B.G. Arden, G.A. Sotzing, *Org. Electron.*, 15 (2014) 1378.
17. S. Liu, X. Zhang, P. Sun, C. Wang, Y. Wei and Y. Liu, *J. Mater. Chem. C.*, 2 (2014) 7891.
18. J.Z. Chen, W.Y. Ko, Y.C. Yen, P.H. Chen and K.J. Lin, *Acs Nano.*, 6 (2012), 6633.
19. M. Zhi, W. Huang, Q. Shi, X. Jia, J. Zhang and S. Zheng, *J. Electrochem. Soc.*, 165 (2018) 804.
20. R.T. Wen, C.G. Granqvist, A.G. Niklasson, *Nat. Mater.*, 14 (2015) 996.
21. B. Balouka, M.A. Arviz, R.T. We, G.A. Niklasson, C.G. Granqvist, R. Vernhes, J.E. Klemberg-Sapieha and L. Martinu, *ACS Appl. Mater. Interfaces.*, 9 (2017) 16995
22. B. Zhang, G. Xu, S. Tan, C. Liu and J. Zhang, *Opt. Mater.*, 100 (2020) 109659.
23. F. Lang, J. Liu, H. Wang and H. Yan, *Nano.*, 12 (2017) 54.
24. S. Zhang, C. Ran, C. Sheng, Y. Gu and B. Yan, *J. Electrochem. Soc.*, 164 (2017) 1021.

© 2021 The Authors. Published by ESG (www.electrochemsci.org). This article is an open access article distributed under the terms and conditions of the Creative Commons Attribution license (<http://creativecommons.org/licenses/by/4.0/>).